

## Helix 8 and the i3 Loop of the Muscarinic M3 Receptor Are Crucial Sites for Its Regulation by the G $\beta$ 5-RGS7 Complex

Darla Karpinsky-Semper,<sup>†</sup> Junior Tayou,<sup>†</sup> Konstantin Levay,<sup>†</sup> Brett J. Schuchardt,<sup>‡</sup> Vikas Bhat,<sup>‡</sup> Claude-Henry Volmar,<sup>§</sup> Amjad Farooq,<sup>‡</sup> and Vladlen Z. Slepak\*,<sup>†</sup>

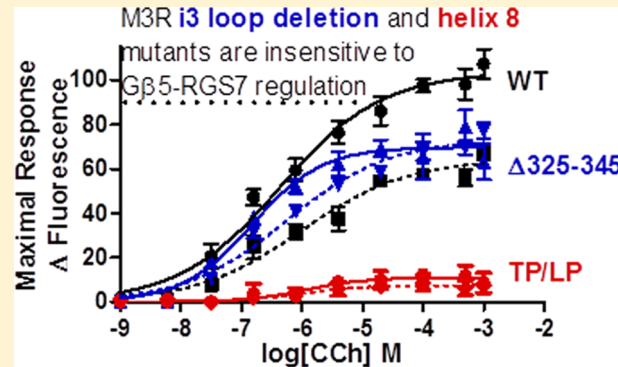
<sup>†</sup>Department of Molecular and Cellular Pharmacology, University of Miami Miller School of Medicine, 1600 NW 10th Avenue, RMSB6024A, Miami, Florida 33136, United States

<sup>‡</sup>Department of Biochemistry and Molecular Biology, University of Miami Miller School of Medicine, 1011 NW 15th Street, #217, Miami, Florida 33136, United States

<sup>§</sup>Department of Psychiatry, University of Miami Miller School of Medicine, 648 Biomedical Research Building, Miami, Florida 33136, United States

**ABSTRACT:** The muscarinic M3 receptor (M3R) is a G $\alpha$ -coupled receptor and is known to interact with many intracellular regulatory proteins. One of these molecules is G $\beta$ 5-RGS7, the permanently associated heterodimer of G protein  $\beta$ -subunit G $\beta$ 5 and RGS7, a regulator of G protein signaling. G $\beta$ 5-RGS7 can attenuate M3R-stimulated release of Ca $^{2+}$  from intracellular stores or enhance the influx of Ca $^{2+}$  across the plasma membrane. Here we show that deletion of amino acids 304–345 from the central portion of the i3 loop renders M3R insensitive to regulation by G $\beta$ 5-RGS7. In addition to the i3 loop, interaction of M3R with G $\beta$ 5-RGS7 requires helix 8. According to circular dichroism spectroscopy, the peptide corresponding to amino acids 548–567 in the C-terminus of M3R assumes an  $\alpha$ -helical conformation.

Substitution of Thr553 and Leu558 with Pro residues disrupts this  $\alpha$ -helix and abolished binding to G $\beta$ 5-RGS7. Introduction of the double Pro substitution into full-length M3R (M3R<sup>TP/LP</sup>) prevents trafficking of the receptor to the cell surface. Using atropine or other antagonists as pharmacologic chaperones, we were able to increase the level of surface expression of the TP/LP mutant to levels comparable to that of wild-type M3R. However, M3R-stimulated calcium signaling is still severely compromised. These results show that the interaction of M3R with G $\beta$ 5-RGS7 requires helix 8 and the central portion of the i3 loop.



The G protein-coupled receptors (GPCRs) respond to a large variety of extracellular signals and make up the largest receptor gene family. The canonical mechanism of signal transduction initiated by GPCRs involves activation of heterotrimeric G proteins, passing the signal onto effector enzymes and ion channels, which in turn regulate the intracellular concentration of second messengers, i.e., cAMP and Ca $^{2+}$ .<sup>1</sup> In addition to G proteins, GPCRs interact with a plethora of molecules, including arrestins, protein kinases, adaptor proteins, PDZ domain-containing proteins, and regulators of G protein signaling (RGS).<sup>2</sup> While interactions with G proteins and arrestins are characteristic of essentially all GPCRs, these other accessory proteins interact with only some GPCRs.

Among the known binding partners of GPCRs are regulators of G protein signaling (RGS) proteins, which are GTPase-activating proteins (GAPs) for G proteins, classically serving as negative regulators of GPCR signaling.<sup>3,4</sup> Approximately 30 mammalian RGS proteins have been identified and are divided among eight subfamilies on the basis of structural similarities.<sup>5</sup> The R7 subfamily of RGS proteins, RGS6, -7, -9, and -11,

uniquely form an obligate heterodimer with the G protein  $\beta$ -subunit  $\beta$ 5 (G $\beta$ 5). All R7 RGS proteins contain an N-terminal DEP (Disheveled, Egl10, and Plekstrin homology) domain, followed by DHEX (DEP Helical EXtension), GGL (G-Gamma-Like), and C-terminal RGS domains. Association of G $\beta$ 5 with the R7-RGS GGL domain stabilizes the heterodimer protecting each protein from degradation.<sup>6,7</sup> The RGS domain harbors its GAP activity, and the DEP domain facilitates membrane targeting and is involved in protein-protein interactions and possibly selectivity.<sup>8–10</sup>

G $\beta$ 5-RGS7 and G $\beta$ 5-RGS9 complexes can interact with some GPCRs, specifically the dopamine D2 receptor (D2R),<sup>11</sup> an orphan receptor GPR158,<sup>12</sup> and the muscarinic M3 receptor (M3R).<sup>6,13–16</sup> There are five muscarinic receptors: in physiological settings, the paradigm is one in which M1, M3, and M5 are coupled to G $\alpha$ q whereas M2 and M4 are coupled to G $\alpha$ i.<sup>17,18</sup> The G $\beta$ 5-RGS7 complex selectively attenuates

Received: August 6, 2014

Revised: December 31, 2014

Published: December 31, 2014

M3R-stimulated  $\text{Ca}^{2+}$  signaling and has no effect on the other muscarinic receptors.<sup>15</sup> Accordingly, the unique third intracellular (i3) loop and cytoplasmic tail (c-tail) of M3R selectively bind to the  $G\beta\gamma$ -RGS7 complex.<sup>15</sup> The i3 loop of M3R is an important region involved in receptor dimerization, G protein recognition, and coupling and interaction with several other proteins.<sup>19–23</sup>

The proximal portion of the carboxyl terminus of M3R contains an  $\alpha$ -helix, which is commonly termed helix 8.<sup>24</sup> To date, structural and biophysical evidence suggests that helix 8 is a common feature that plays an important role in GPCR localization and signal transduction.<sup>25–30</sup> The conformational dynamics of helix 8 has been shown to be dependent on the ligand and binding partner.<sup>29,31</sup> In this study, we used protein interaction analysis, spectroscopy, and signaling assays to delineate the structural basis of M3R signal transduction regulation by the  $G\beta\gamma$ -RGS7 complex.

## EXPERIMENTAL PROCEDURES

**Reagents and Antibodies.** Fluo-8 and fura2-AM were from Abcam and Life Technologies, respectively. All other reagents were purchased from Sigma-Aldrich, unless otherwise stated. Rabbit antibody for  $G\beta\gamma$  (1:1000 WB and 1:300 IF) was described previously (REF). Mouse anti-GFP antibody JL-8 was from Clontech (1:3000 WB and 1:1000 IF), and anti-rabbit (1:5000) and anti-mouse (1:3000) secondary antibodies conjugated to horseradish peroxidase were from Jackson Laboratories. Anti-rabbit fluorescein-labeled antibodies (1:400) were from Amersham Biosciences, and the anti-mouse Cy3-labeled antibody (1:400) was from Sigma-Aldrich.

**Cloning and Purification of GST-M3R Constructs.** All constructs were cloned into the pGEX-2T vector (GE Healthcare) at *Bam*H I and *Eco*R I sites. The GST fusions (GST-M3CT-K → A, GST-M3CT-CT, GST-M3CT-NT, and GST-M3CT-TP/LP) were made by polymerase chain reaction (PCR) mutagenesis and verified by sequencing. GST fusion proteins were expressed in *Escherichia coli* and purified on glutathione beads using a standard protocol described previously.<sup>16</sup> Briefly, 1 L bacterial cultures were grown to an OD<sub>600</sub> of 1.0 at 37 °C. Protein expression was induced with the addition of 0.4 mM IPTG for 1.5–2 h at 30 °C. Cells were pelleted and stored at –80 °C until they were used further. Pellets were resuspended in BugBuster Master Mix lysis buffer (Novagen) supplemented with protease inhibitors (Complete, Roche). Protein solubilization was achieved by adding the ionic detergent *N*-lauroylsarcosine to a concentration of 1.5% for 10 min at room temperature. *N*-Lauroylsarcosine was sequestered by Triton X-100 (final concentration of 2%), and the lysate was centrifuged at 19000 rpm and 4 °C for 30 min. Glutathione-Sepharose 4B beads (GE) were incubated with lysate for 2 h and washed with PBS. Bound GST fusion proteins were eluted with 20 mM glutathione, desalted on Sephadex G-25 pre-equilibrated with buffer containing 100 mM Tris-HCl (pH 8.0), 150 mM NaCl, and 15% glycerol, and stored frozen in aliquots at –80 °C. The protein concentration was determined using the Bio-Rad protein assay kit according to the manufacturer's recommendations with bovine serum albumin as a standard. The concentration of the frozen GST-M3R protein stock was 2.5 mg/mL (~65  $\mu$ M). The purity of GST was >90% as determined by sodium dodecyl sulfate–polyacrylamide gel electrophoresis.

**Constructs for Expression in Mammalian Cells.** Constructs encoding  $G\beta\gamma$  and RGS7 genes were previously

described.<sup>16</sup> The constructs encoding the human muscarinic M3 receptor gene (M3R) and an N-terminal HA-tagged M3R (HA-M3R) in a pcDNA3.1 vector were purchased from cDNA.org. These constructs were used for subsequent cloning of M3R and HA-M3R mutants [M3R<sup>Δ304–390</sup>, M3R<sup>Δ304–325</sup>, M3R<sup>Δ324–345</sup>, M3R<sup>Δ370–390</sup>, and M3R<sup>TP/LP</sup> (see the text)] utilizing PCR mutagenesis techniques.

**Cell Culture and Transfection.** Chinese hamster ovary (CHO-K1) cells were cultured in F-12K medium with 10% fetal bovine serum and penicillin/streptomycin. Twenty-four hours prior to transfection, cells were seeded on 12 mm glass coverslips, 10 cm plates, or 6-well plates, as required by the experiment, to achieve 50–75% confluence at the time of transfection. Lipofectamine2000 transfection reagent (Life Technologies) was used according to the manufacturer's guidelines at a 2:1 reagent:DNA ratio. The total amount of DNA for 12 mm coverslip transfections was 0.5  $\mu$ g and was scaled up according to the relative surface for transfection in larger vessels. The ratio of  $G\beta\gamma$  to RGS7 was always 1:3, and for cotransfection with M3R and  $G\beta\gamma$ -RGS7, the DNA ratio was 1:1:3. Empty pcDNA3.1 or LacZ plasmid DNA was used to ensure constant DNA loading in cotransfections. Forty-eight hours after transfection, cells were used for  $\text{Ca}^{2+}$  imaging or immunofluorescence studies. For GST pull-down assays, cells were washed in ice-cold PBS and scraped in a hypotonic lysis buffer containing 20 mM Tris-HCl, 5 mM NaCl<sub>2</sub>, 1 mM MgCl<sub>2</sub>, 2 mM CaCl<sub>2</sub>, 1 mM DTT, 1 mM EDTA, 1 mM EGTA, and protease inhibitors, followed by two freeze–thaw cycles at –80 °C and centrifugation for 45 min at 4 °C and 20000g. The resulting supernatant was collected and used in the GST pull-down assay. Fresh lysate was prepared for each experiment.

**GST Pull-Down Assay.** As previously described,<sup>16</sup> Glutathione-Sepharose 4B beads were prewashed with PBS and 0.1% CHAPS, incubated at 4 °C with purified recombinant GST or the GST fusion proteins for 1 h, and washed three times with PBS and 0.1% CHAPS to remove excess protein. The slurry was incubated for 1–2 h at 4 °C on a rotary shaker with the various lysates as determined by the experiment. At the end of the incubation, the beads settled because of gravity, and the supernatant was collected as the unbound fraction. The resin was extensively washed and subsequently eluted with the addition of sodium dodecyl sulfate (SDS)-containing sample loading buffer. In a typical assay, the packed volume of the GST resin was 30  $\mu$ L, the amount of loaded GST fusion protein was 10  $\mu$ g, and the volume of the protein lysate was 300  $\mu$ L. The total protein concentration in transfected cell lysates was 2.5–5.0 mg/mL. The beads were washed three times with 600  $\mu$ L of PBS and 0.1% CHAPS buffer and eluted with 30  $\mu$ L of 2× SDS sample loading buffer. The unbound and eluted fractions were resolved by gel electrophoresis and analyzed by Western blotting with chemiluminescent detection. Films were scanned, and densitometric measurements of the bands were calculated using ImageJ.

**Immunofluorescence.** Transfected CHO-K1 cells grown on glass coverslips were fixed with 4% paraformaldehyde and incubated for 30 min a blocking buffer containing 1% BSA in PBS with or without 0.1% Triton X-100, as determined by the experiment. Antibodies were diluted in blocking buffer and incubated with fixed cells for 30 min each with three washes with PBS between and after antibody incubations. Coverslips were affixed to glass slides using ProLong Gold Antifade with DAPI (Life Technologies). After drying overnight, slides were ready for imaging.

**Flow Cytometry.** For the analysis of M3R surface expression, transfected CHO-K1 cells were rinsed with PBS and detached by incubation with 1 mM EGTA and 5 mM EDTA in PBS. After cells were washed once in 1 mL of staining buffer [PBS (pH 7.2), 0.5% BSA, and 2 mM EDTA], they were resuspended in 100  $\mu$ L of staining buffer with 10  $\mu$ L of mouse anti-HA phycoerythrin-conjugated antibody (130-092-257, Miltenyi Biotec GmbH) and incubated for 10 min in the dark (8 °C). Cells were washed in 2 mL of staining buffer by centrifugation at 300g for 5 min and resuspended in 1 mL of 0.5% formaldehyde in PBS. Flow cytometry was performed using a Becton Dickinson LSR II instrument with 10000 events acquired per sample.

**Ca<sup>2+</sup> Imaging Microscopy.** As previously described,<sup>13</sup> transiently transfected CHO-K1 cells grown on 12 mm glass coverslips were washed with culture medium and then incubated at 37 °C in culture medium containing 2  $\mu$ M fura2-AM for 25 min. After fura2-AM loading, the cells were kept at ambient temperature for no longer than 1.5 h before being imaged. Coverslips were secured in a flow chamber and mounted on the stage of a Nikon TE2000 inverted fluorescence microscope. The cells were continuously superfused by gravity flow with HBSS either with or without CaCl<sub>2</sub> and MgCl<sub>2</sub> (Life Technologies). As required by the experiment, the flow was switched to agonist-containing HBSS for a specified time and then changed back to agonist-free buffer. Images were collected in real time every 3 s using a 20× UV objective lens and recorded using Metafluor software. The excitation wavelengths were 340 nm (Ca<sup>2+</sup>-bound) and 380 nm (Ca<sup>2+</sup>-free), and the emission was set to 510 nm. The 340 nm:380 nm ratio is representative of the intracellular free Ca<sup>2+</sup> concentration. The entire field of view was selected as a region of interest (ROI). A typical ROI contained 50–70 cells, of which 30–50 were YFP-positive. The number of cells responding to muscarinic agents varied with agonist concentration but was typically 25–35 in a particular ROI. Traces shown here are averages of two to four independent experiments with three replicate coverslips per experiment.

**FLIPR Ca<sup>2+</sup> Imaging.** Cells were transfected in 10 cm dishes. At 24 h post-transfection, cells were seeded in a black-walled 384-well plate at a density of 10000 cells/well. The Fluo-8 No Wash Calcium Assay kit (Abcam, ab112129) was used according to the manufacturer's recommendations. With this system, there is no washing step after incubation with the Ca<sup>2+</sup> indicator as there is a quenching dye that is not membrane permeant, thus reducing the signal of the extracellular dye. Briefly, growth medium was removed, and cells were washed with Ca<sup>2+</sup>-free HHBSS (20 mM Hepes in Hanks balanced salt solution). A 2× solution of the Fluo-8 dye was prepared in Ca<sup>2+</sup>-free HHBSS and 1% pluronic acid. Equal volumes of HHBSS and Fluo-8 were added to the cells and placed in the 37 °C incubator for 30 min. The plate was then allowed to equilibrate to atmospheric conditions for 20 min before being analyzed with the FLIPR Tetra system. A baseline read of plate fluorescence of 10 s was performed prior to the addition of agonist. After agonist application, the fluorescence intensity was recorded every second for at least 3 min.

**[<sup>3</sup>H]NMS Binding Assay.** The muscarinic receptor density was determined by the ligand binding assay using the muscarinic antagonist *N*-methyl scopolamine chloride ([<sup>3</sup>H]NMS, 84.1 Ci/mmol, PerkinElmer) essentially as previously described.<sup>15</sup> Briefly, CHO-K1 cells were transfected in 10 cm dishes with wild-type or mutant M3R. Twenty-four

hours after transfection, cells were detached and seeded in 24-well plates at a density of 100000 cells/well, at which time atropine was added where required by the experiment. One day after, cells were washed and incubated with 1 mL of [<sup>3</sup>H]NMS in HBSS for 30 min at room temperature. The [<sup>3</sup>H]NMS concentration was 50 nM. Following the incubation, cells were rapidly washed twice with 1 mL of ice-cold buffer and then lysed with 0.25 mL of 0.1 M NaOH added to the wells. This lysate was neutralized with 0.25 mL of 0.1 M HCl; 0.5 mL of 50 mM Hepes (pH 7.2) was added, and the mixture was transferred to the vials for liquid scintillation counting. Triplicate wells were used for each experimental condition. Nonspecific binding was assessed using mock-transfected cells.

**cAMP Assay.** We used the LANCE Ultra cAMP competitive immunoassay kit (PerkinElmer); 5000 cells were seeded in 10  $\mu$ L of cell buffer (HBSS, 25 mM Hepes, and 0.1% BSA) onto 384-well microtiter plates. Then, 5  $\mu$ L of test compound prepared in assay buffer (0.1% BSA, 25 mM Hepes, and 500  $\mu$ M 3-isobutyl-1-methylxanthine) or buffer alone was added to the appropriate wells, and plates were incubated at room temperature for 30 min. After this incubation, 5  $\mu$ L of Eu-cAMP (prepared in lysis buffer according to the manufacturer's protocol) followed by 5  $\mu$ L of ULight-labeled anti-cAMP in the same buffer was added to each well and incubated for 1 h at room temperature. FRET measurements were performed using the Envision microplate reader (PerkinElmer) at the following wavelengths: 340 nm (with a 30 nm bandwidth) excitation and 671 nm (with a 4 nm bandwidth) emission.

**Peptide Synthesis.** 20-mer wild-type (WT) and mutant (TP/LP) peptides corresponding to the C-terminal tail (residues 548–567) of M3R were commercially obtained from GenScript Corp. The amino acid sequences of these peptides were 548-NKTFRTFKMLLCQCDKKK-567 (WT) and 548-NKTFRPTFKMPLLCQCDKKK-567 (TP/LP). Note that residues T553 and L558 and their proline counterparts are depicted in bold font. The peptide concentrations were measured gravimetrically.

**Circular Dichroism.** Far-UV circular dichroism (CD) measurements were conducted on a Jasco J-815 spectropolarimeter thermostatically controlled at 25 °C. Briefly, 20-mer WT and TP/LP peptides were dialyzed in 10 mM sodium phosphate (pH 7.0), and experiments were conducted on a 50  $\mu$ M sample of each peptide alone in solution or in the presence of 5 mM *n*-dodecylphosphocholine (DPC) bicelles (Avanti Polar Lipids). The DPC bicelles were prepared at a stock concentration of 10 mM in 10 mM sodium phosphate (pH 7.0) by being stirred for 2 h at 37 °C. Data were collected using a quartz cuvette with a 2 mm path length in the 185–255 nm wavelength range and with a slit bandwidth of 2 nm at a scan rate of 10 nm/min. All data were normalized against reference spectra to remove the contribution of buffer. Each data set represents an average of four scans acquired at 0.1 nm intervals. Data were converted to mean ellipticity,  $[\theta]$ , as a function of wavelength ( $\lambda$ ) of electromagnetic radiation using the following equation:

$$[\theta] = [(10^5 \Delta \epsilon)/cl] \text{ deg cm}^2 \text{ dmol}^{-1}$$

where  $\Delta \epsilon$  is the observed ellipticity in millidegrees,  $c$  is the peptide concentration in micromolar, and  $l$  is the cuvette path length in centimeters.

**Molecular Modeling.** Structural models of WT and TP/LP peptides (residues 548–567) were built using the MODELER software based on homology modeling.<sup>32</sup> In each case, the

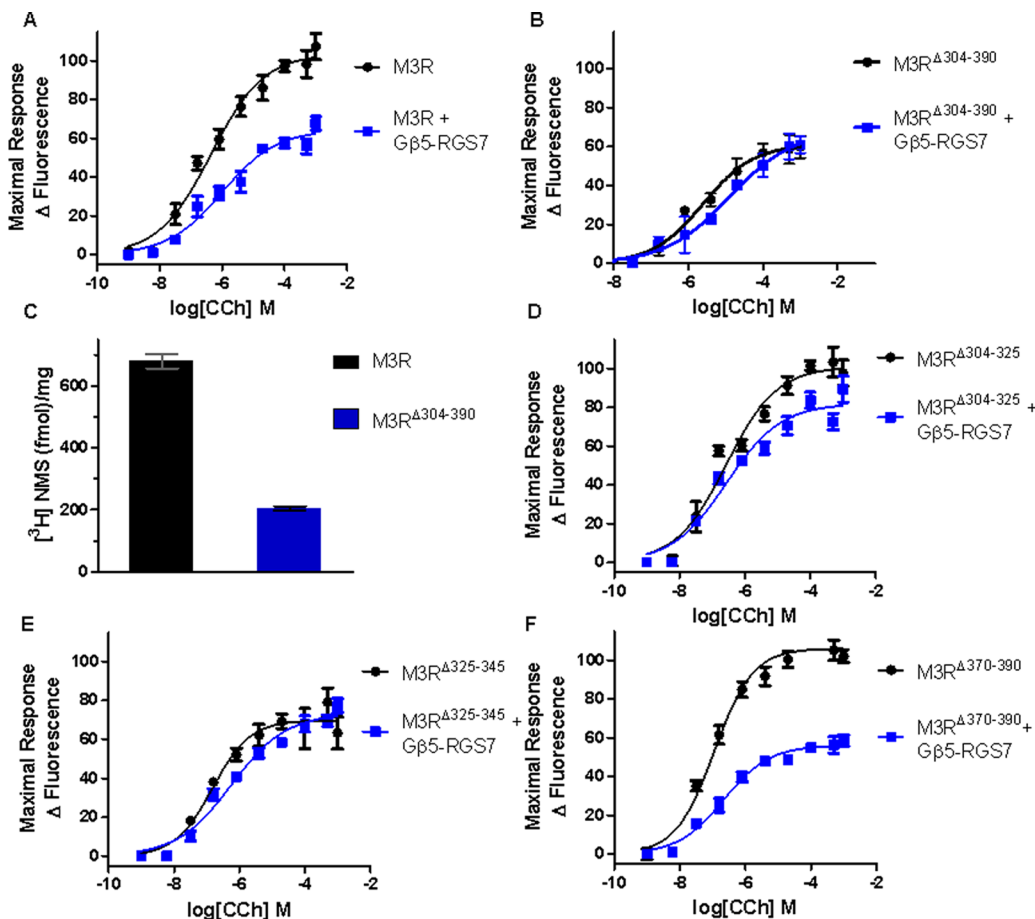


**Figure 1.** M3R i3 loop deletions abolish its sensitivity to G $\beta$ 5-RGS7 regulation. CHO-K1 cells were transiently transfected with WT M3R or the i3 loop deletion mutants (M3R<sup>Δ</sup>304–325, M3R<sup>Δ</sup>325–345, M3R<sup>Δ</sup>370–390, and M3R<sup>Δ</sup>304–390) in the presence or absence of G $\beta$ 5-RGS7 and prepared for Ca<sup>2+</sup> imaging using FLIPR as described in Experimental Procedures. Concentration dependencies of the maximal change in Fluo-8 fluorescence from cells expressing WT M3R (A), M3R<sup>Δ</sup>304–390 (B), M3R<sup>Δ</sup>304–325 (D), M3R<sup>Δ</sup>325–345 (E), and M3R<sup>Δ</sup>370–390 (F) in the absence (black) and presence (blue) of G $\beta$ 5-RGS7 stimulated by CCh. Each data point is the mean  $\pm$  the standard error of the mean of four replicate wells from two independent experiments. Curves were fit using the GraphPad Prism 5 sigmoidal dose–response equation with a variable slope and normalized to the maximal response from cells expressing WT M3R in the absence of G $\beta$ 5-RGS7. (C) [<sup>3</sup>H]NMS binding to WT M3R and M3R<sup>Δ</sup>304–390 performed on live cells as described in Experimental Procedures. Bar graphs show means  $\pm$  SD ( $n = 2$ ).

crystal structure of the CHRM3 receptor (Protein Data Bank entry 4DAJ) harboring helix H8 (residues 548–556) was used as a template.<sup>24</sup> For each peptide, a total of 100 atomic models were calculated, and the structure with the lowest energy, as judged by the MODELER Objective Function, was selected for further analysis. The structural models were rendered using RIBBONS.<sup>33</sup>

**Molecular Dynamics.** Molecular dynamics (MD) simulations were performed with GROMACS<sup>34</sup> using the integrated AMBER99SB-ILDN force field.<sup>35,36</sup> Briefly, the structural models of WT and TP/LP peptides (residues 548–567) were each centered in a cubic box and explicitly hydrated with a water layer that extended 10 Å (box size) from the protein surface along each orthogonal direction using the extended simple point charge (SPC/E) water model.<sup>37,38</sup> The ionic strength of the solution was set to 100 mM with NaCl, and the hydrated structures were energy-minimized with the steepest descent algorithm prior to equilibration under the NPT ensemble conditions, wherein the number of atoms (N), pressure (P), and temperature (T) within the system were kept constant. The particle mesh Ewald (PME) method<sup>39</sup> was employed to compute long-range electrostatic interactions with a spherical cutoff of 10 Å and a grid space of 1.6 Å with a

fourth-order interpolation. The linear constraint solver (LINCS) algorithm was used to restrain bond lengths.<sup>40</sup> All MD simulations were performed at 300 K under periodic boundary conditions (PBC), to mimic the bulk solvent effect, using the standard “md” leapfrog integrator to solve Newton’s equations of motion with a time step of 2 fs. For the final MD production runs, data were collected every nanosecond over a time scale of 1  $\mu$ s. All MD simulations were performed on a Linux workstation using parallel processors at the High Performance Computing (HPC) facility within the Center for Computational Science (CCS) of the University of Miami.

## RESULTS

**Residues 304–345 of the i3 Loop of M3R Are Required for Its Regulation by G $\beta$ 5-RGS7.** To extend our earlier finding that the M3R i3 loop is required for the interaction with G $\beta$ 5-RGS7,<sup>15</sup> we created and analyzed several deletion mutants in this region (Figure 1). First, we studied deletion of amino acids 304–390, which were previously identified by a GST pull-down assay as the region involved in the interaction with G $\beta$ 5-RGS7.<sup>15</sup> Deletion of this region within the full-length receptor (M3R<sup>Δ</sup>304–390) was tested for sensitivity to G $\beta$ 5-RGS7 in the CCh-stimulated Ca<sup>2+</sup> signaling

Table 1. Effects of i3 Loop Deletions on the Sensitivity of M3R to G $\beta$ 5-RGS7<sup>a</sup>

	M3R			M3R with G $\beta$ 5-RGS7		
	n <sup>b</sup>	E <sub>max</sub> <sup>c,d</sup>	-log EC <sub>50</sub> <sup>d,e</sup>	n <sup>b</sup>	E <sub>max</sub> <sup>c,d</sup>	-log EC <sub>50</sub> <sup>d,e</sup>
WT	80	100 ± 3.94	6.35 ± 0.13	86	64 ± 3.15	6.00 ± 0.16
M3R $^{\Delta 304-325}$	60	101 ± 3.66	6.57 ± 0.14	67	82 ± 3.11	6.56 ± 0.13
M3R $^{\Delta 325-345}$	63	70 ± 2.78	6.82 ± 0.13	67	73 ± 2.37	6.24 ± 0.11
M3R $^{\Delta 370-390}$	64	106 ± 2.62	6.95 ± 0.08	67	56 ± 1.60	6.66 ± 0.10
M3R $^{\Delta 304-390}$	36	61 ± 4.05	5.61 ± 0.23	36	68 ± 10.33	4.90 ± 0.43

<sup>a</sup>CCh-induced Ca<sup>2+</sup> signaling was measured by FLIPR in cells transfected with different M3R i3 loop deletion mutants as described in the legend of Figure 1 and Experimental Procedures. <sup>b</sup>n is the number of points analyzed (two independent experiments). <sup>c</sup>E<sub>max</sub> is the maximal change in well fluorescence expressed as a percentage of that of WT M3R (=100%). <sup>d</sup>Mean ± the standard error of the mean. <sup>e</sup>-Log EC<sub>50</sub> (in molar) is the negative logarithm of the agonist concentration that produces the half-maximal effect.

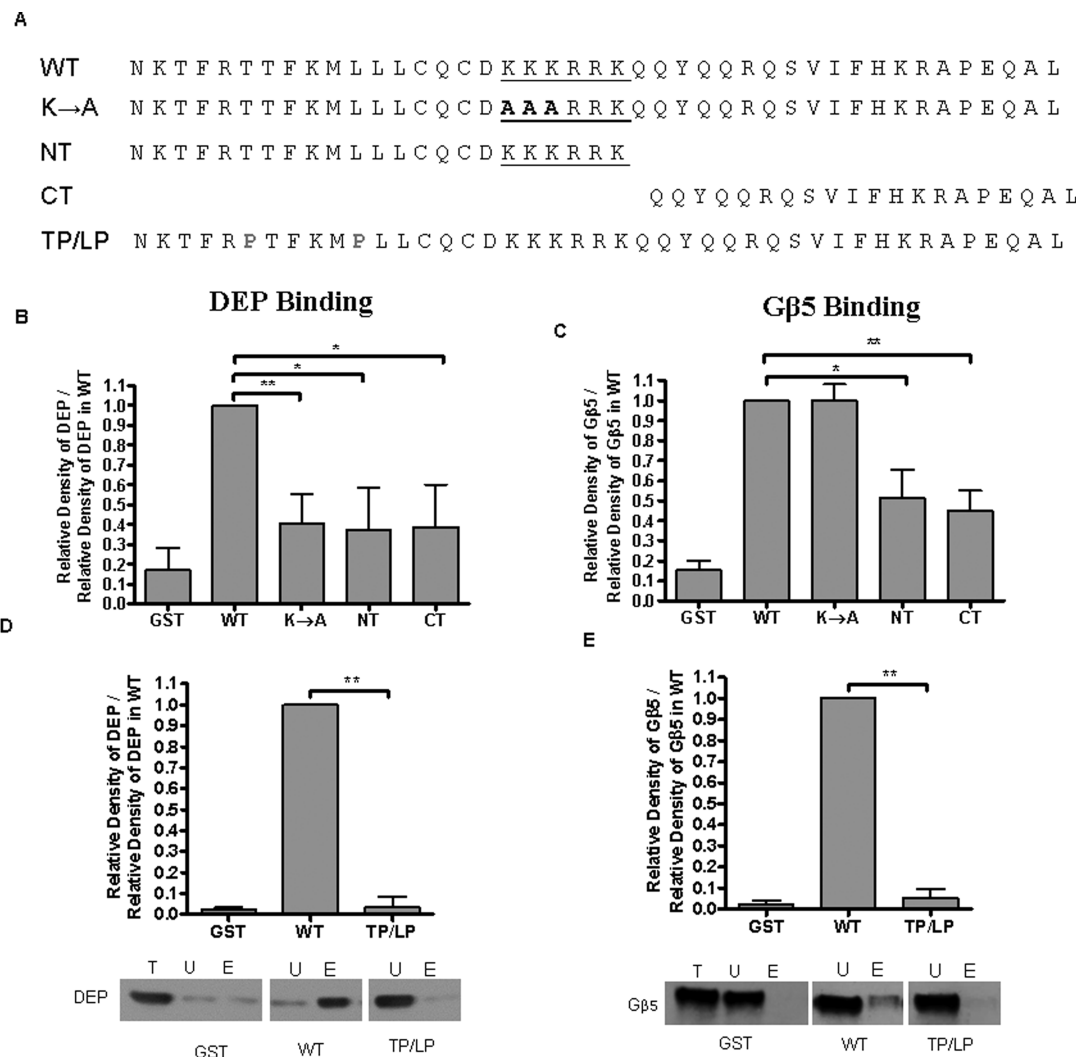


**Figure 2.** M3R helix 8 is essential for interaction with G $\beta$ 5-RGS7. Four GST fusion proteins of the M3R CT were purified from bacteria and tested for interaction with G $\beta$ 5-RGS7 in a pull-down assay as described in Experimental Procedures. (A) Amino acid sequences of M3R C-tail GST fusion proteins. The polybasic region is underlined; the substituted Lys-to-Ala residues are shown in bold (K → A), and the truncated fusions are designated as NT and CT. The positions of the two residues, T553 and L558, substituted with Pro are colored red. Purified GST fusions were immobilized on glutathione-Sepharose 4B beads. To analyze the interaction with the DEP domain, lysates from CHO-K1 cells expressing YFP-DEP were applied to protein-coated beads. For G $\beta$ S, constructs encoding G $\beta$ S and RGS7<sup>R249</sup>, RGS7 without the DEP domain, were cotransfected to stabilize the G $\beta$ S protein. The total (T), unbound (U), and eluted (E) material was analyzed by Western blotting using antibodies against YFP or G $\beta$ S for DEP or G $\beta$ S detection, respectively. Resulting blots were scanned, and the band density was quantified using ImageJ. (B and D) Average relative density ± SD (n = 3) of DEP detected in each sample normalized to the relative density of DEP in the eluted fraction in the pull down using the WT C-tail. (C and E) Quantification of the average relative density ± SD (n = 3) of eluted G $\beta$ S in each sample normalized to the relative density of the G $\beta$ S band in the WT sample.

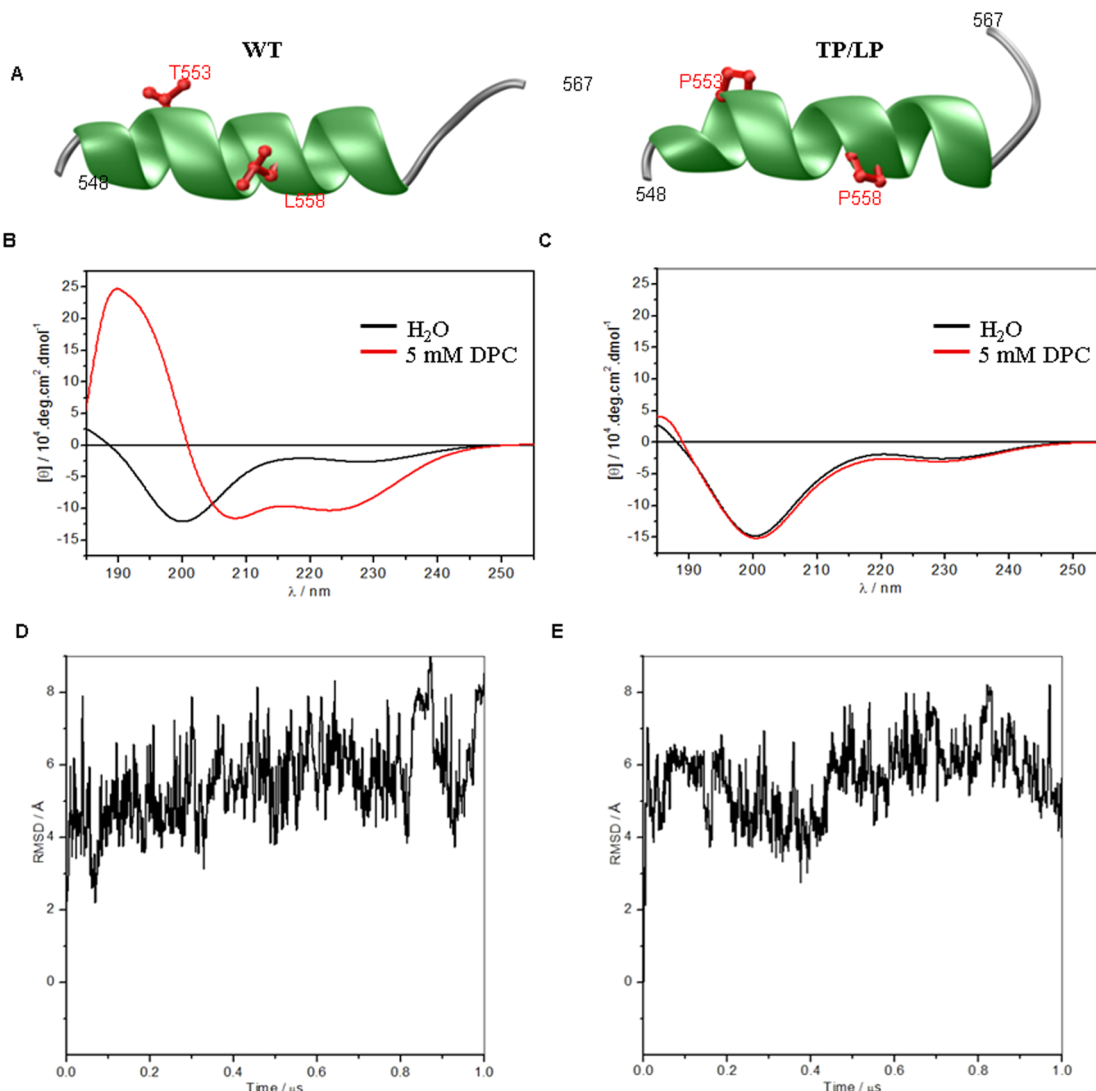


**Figure 3.** *In silico* and biophysical analysis of M3R helix 8. (A) Ribbon representation of the structural models of helix 8 of WT (left) and TP/LP peptides (right). For each structural model, helix 8 is colored green, the terminal loops are colored gray, and the side chain moieties of T553/L558 residues and their proline counterparts are colored red. (B) Far-UV spectra of the WT peptide (40  $\mu$ M) in the absence (black) and presence (red) of 5 mM DPC. (C) Far-UV spectra of the TP/LP peptide (40  $\mu$ M) in the absence (black) and presence (red) of 5 mM DPC. (D and E) Molecular dynamics simulations for each peptide. Root-mean-square deviations (rmsd) of backbone atoms (N, Ca, and C) within each simulated structure relative to the initial modeled structure of helix 8 of M3R WT (D) and TP/LP (E) as a function of simulation time are shown.

assay. Consistent with previous findings,<sup>13,15,41</sup> G $\beta$ 5-RGS7 reduced the  $E_{\max}$  of the M3R-stimulated Ca<sup>2+</sup> response to 65% of that of M3R alone (Figure 1A), with little effect on EC<sub>50</sub> (Table 1). In contrast, G $\beta$ 5-RGS7 could not attenuate CCh-stimulated Ca<sup>2+</sup> responses from the M3R<sup>Δ304–390</sup> mutant (Figure 1B). Compared to that of WT M3R, the  $E_{\max}$  from M3R<sup>Δ304–390</sup> was reduced by ~30%; however, the EC<sub>50</sub> remained unchanged. These results indicate that deletion of residues 304–390 did not alter the affinity of CCh for M3R (no change in EC<sub>50</sub>) but reduced the level of surface expression and/or coupling to Gq (reduced  $E_{\max}$ ) and abolished attenuation by G $\beta$ 5-RGS7. Indeed, quantification of [<sup>3</sup>H]NMS binding on intact cells overexpressing M3R<sup>Δ304–390</sup> showed that its level was lower than that of WT by 60% (Figure 1C). Nevertheless, the dynamic range of Ca<sup>2+</sup> responses elicited by M3R<sup>Δ304–390</sup> is sufficient to detect inhibition, so our results clearly show that residues 304–390 of the i3 loop are required for the negative effect of G $\beta$ 5-RGS7.

Recently, we found that the G $\beta$ 5-RGS7 complex has a dual effect on M3R-stimulated Ca<sup>2+</sup> signaling: while it inhibits the release of Ca<sup>2+</sup> from intracellular stores, it can also augment the influx of Ca<sup>2+</sup> across the plasma membrane.<sup>13</sup> Here, we found that both Ca<sup>2+</sup> release and influx components were insensitive to G $\beta$ 5-RGS7 regulation in the M3R<sup>Δ304–390</sup> mutant (data not shown), indicating that the region of residues 304–390 of M3R is required for G $\beta$ 5-RGS7-mediated modulation of both Ca<sup>2+</sup> entry pathways.

Analysis of three shorter deletions, M3R<sup>Δ304–325</sup>, M3R<sup>Δ325–345</sup>, and M3R<sup>Δ370–390</sup>, showed that removal of amino acids 304–325 or 325–345 reduced the sensitivity of M3R to the G $\beta$ 5-RGS7 complex by 18 or 27%, respectively (Figure 1D–F and Table 1). The deletion of residues 370–390 did not reduce the sensitivity to G $\beta$ 5-RGS7 but, interestingly, slightly enhanced attenuation of the Ca<sup>2+</sup> response by G $\beta$ 5-RGS7. The three smaller i3 loop deletions did not appear to affect receptor surface expression, as the  $E_{\max}$  was similar to that

of WT M3R (Table 1). Altogether, these experiments have narrowed down the G $\beta$ 5-RGS7-sensitizing region of the i3 loop of M3R to residues 304–345.

**Integrity of M3R C-Terminal Secondary Structure Is Required for Its Interaction with G $\beta$ 5-RGS7.** Previous studies in our laboratory revealed that along with the i3 loop, regulation by G $\beta$ 5-RGS7 involves the C-terminus of M3R, with both G $\beta$ 5 and DEP moieties binding to the recombinant M3R C-tail *in vitro*.<sup>14</sup> To gain insights into the structural features of the C-tail required in this interaction, we generated four GST fusions of the C-tail and tested them in a pull-down assay with the G $\beta$ 5-RGS7 complex (Figure 2). First, we first focused on a unique polybasic sequence, S65-KKKRRKK-570 in the middle of the C-tail, which was identified as a region necessary for anti-apoptotic effects of the M3R<sup>42</sup> and a site of Gq heterotrimer preassembly.<sup>43</sup> In the GST-M3CT K → A construct, the first three Lys residues were replaced with Ala (Figure 2A). We also made two smaller fragments, GST-M3CT NT, which contained the polybasic region, and M3CT CT, which contained the remaining C-tail (Figure 2A). As previously described,<sup>15,16</sup> we used lysates from CHO-K1 cells overexpressing YFP-DEP or G $\beta$ 5 complex with the RGS7<sup>R249</sup> construct missing the DEP and DHEX domains, to probe for interaction of DEP or G $\beta$ 5 with the GST fusions, respectively. YFP-DEP exhibited a reduced level of binding to all three GST fusions as compared to that of the full-length C-tail (Figure 2B). For G $\beta$ 5 interaction, both the NT and CT fragments exhibited reduced levels of binding (Figure 2C). Thus, the entire C-tail including the polybasic stretch is essential for interaction with the G $\beta$ 5-RGS7 complex. Next, we explored whether the secondary structure of the C-tail could be important for its interaction with the G $\beta$ 5-RGS7 complex.

Crystallographic analysis of M3R confirms that the proximal region of its C-tail adopts an  $\alpha$ -helical conformation, commonly termed helix 8.<sup>24</sup> To test the idea that G $\beta$ 5-RGS7 binding is dependent on the secondary structure of helix 8, we introduced two Pro residues in place of Thr and Leu at positions 553 and 558, respectively. We then expressed this mutant, TP/LP, as a GST fusion protein. We found that the TP/LP mutation nearly abolished binding of the recombinant M3R C-tail to both DEP (Figure 2D) and G $\beta$ 5 (Figure 2E).

#### Biophysical Analysis of Pro-Substituted M3R Helix 8.

To understand if the TP/LP mutation indeed affects secondary structure, we conducted far-UV CD analysis on 20-mer wild-type and mutant (TP/LP) peptides spanning helix 8 (Figure 3B,C). Our analysis reveals that the spectra of both WT and TP/LP peptides in aqueous solution are characterized by a negative band centered around 200 nm (Figure 3B), characteristic of peptides predominantly harboring random coil conformation.<sup>44,45</sup> However, in the membrane-like environment of DPC bicelles, the WT peptide spectrum exhibits a positive band centered around 190 nm and two negative bands around 208 and 222 nm (Figure 3C, red line). Such a spectral signature is a hallmark of  $\alpha$ -helical peptides, which strongly suggests that the WT peptide adopts an  $\alpha$ -helical conformation in an apolar membrane-like environment. In sharp contrast, the addition of DPC bicelles to the TP/LP peptide does not alter its spectrum (Figure 3C, black line), implying that double Pro substitution disrupts the  $\alpha$ -helix.

We modeled the structures of WT and TP/LP peptides and conducted molecular dynamics simulations in water solvent (Figure 3D,E). Interestingly, our MD analysis reveals that the WT peptide reaches structural equilibrium with a root-mean-

square deviation (rmsd) of  $\sim$ 7 Å (Figure 3D), implying that it is extremely unstable in water because of its intrinsic structural flexibility. This observation is consistent with our CD data showing that the WT peptide adopts a random coil conformation in aqueous solution and becomes  $\alpha$ -helical only in the presence of an apolar membrane. Likewise, the stability of the TP/LP peptide in water is comparable to that of the WT peptide (Figure 3E).

**Helix 8 Is Required for M3R Trafficking, Signaling, and G $\beta$ 5-RGS7 Interaction.** Next, we introduced the TP/LP mutation into the full-length M3R (M3R<sup>TP/LP</sup>) and tested its sensitivity to G $\beta$ 5-RGS7 in the Ca<sup>2+</sup> signaling assay (Figure 4).

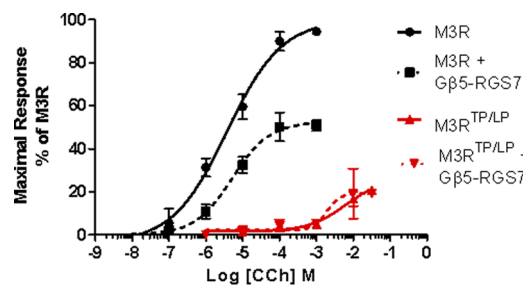


**Figure 4.** CCh-stimulated Ca<sup>2+</sup> signaling is severely impaired by the M3R<sup>TP/LP</sup> mutation. Concentration dependencies of the maximal Ca<sup>2+</sup> response of WT M3R (black) or M3R<sup>TP/LP</sup> (red) in the absence (dashed lines) or presence (solid lines) of G $\beta$ 5-RGS7 stimulated by CCh using fura2, as described in Experimental Procedures. Each data point is the average  $\pm$  SD of three coverslips from two independent experiments ( $n = 6$ ). Curves were fit using the GraphPad Prism 5 sigmoidal dose-response equation with variable slope.

Ca<sup>2+</sup> responses to CCh were nearly undetectable in cells transfected with the M3R<sup>TP/LP</sup> mutant. Because helix 8 is necessary for GPCR trafficking<sup>46–48</sup> we compared the subcellular localization of M3R<sup>TP/LP</sup> to that of WT M3R. Radioligand binding studies (Figure 5A) and immunological detection of the HA-tagged receptor (Figure 6) revealed that surface expression of M3R<sup>TP/LP</sup> was severely compromised.

It is known that membrane-permeable antagonists can act as pharmacological chaperones, improving surface expression of helix 8 mutants of muscarinic M1<sup>49</sup> and vasopressin V2<sup>50</sup> receptors. This effect involves stabilization of the mutant receptor in the endoplasmic reticulum, allowing it to pass quality control of the secretory pathway.<sup>51</sup> Here, to facilitate trafficking of M3R<sup>TP/LP</sup>, we applied the pharmacological chaperone approach pretreating cells with the membrane-permeable muscarinic antagonist atropine. We found that atropine treatment greatly enhanced [<sup>3</sup>H]NMS binding in cells expressing M3R<sup>TP/LP</sup> from <2 to  $\sim$ 50% of WT (Figure 5). Similarly, quantification of cell surface expression of HA-M3R using flow cytometry showed that pharmacological chaperone treatment led to a dramatic increase in the level of M3R<sup>TP/LP</sup> trafficking (Figure 6). It is worth mentioning that atropine also increased the level of [<sup>3</sup>H]NMS binding in cells expressing i3 loop mutant M3R<sup>Δ304–390</sup> by approximately 2-fold (data not shown).

We also tested if other structurally diverse muscarinic antagonists such as scopolamine, dicyclomine, and pirenzipine were capable of acting as a pharmacological chaperone (Figure 5). We found that cell surface expression of M3R<sup>TP/LP</sup>, as detected by [<sup>3</sup>H]NMS binding (Figure 5A), was enhanced by incubation with each antagonist utilized in this study. It is

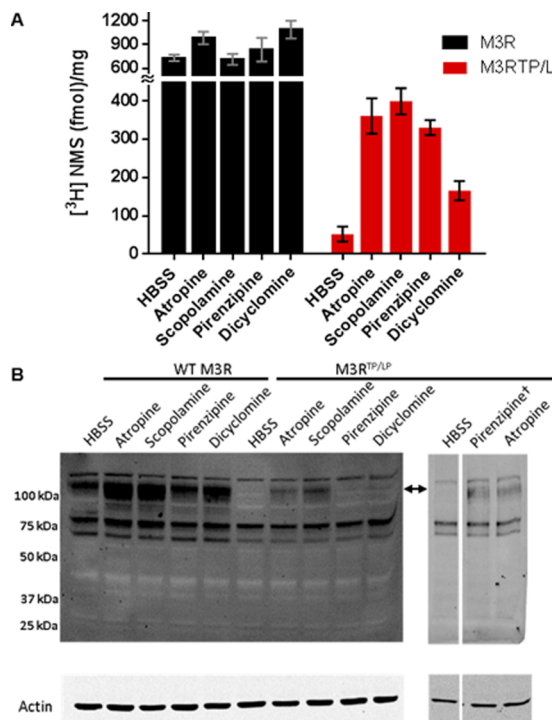


**Figure 5.** Muscarinic antagonists act as pharmacological chaperones for the M3R<sup>TP/LP</sup> mutant. (A)  $[^3\text{H}]$ NMS binding to WT M3R (black bars) and M3R<sup>TP/LP</sup> (red bars) was performed on live cells as described in Experimental Procedures. Antagonists were added to cells for 18 h and washed away prior to incubation with  $[^3\text{H}]$ NMS. All antagonists were used at the final medium concentration of 100 nM, except for pirenzepine, which was used at a concentration of 200  $\mu\text{M}$ . Bar graphs show means  $\pm$  SD ( $n = 2$ ). (B) Representative Western blots of cells treated with the indicated antagonists at a concentration of 100 nM. The separate right panel shows cells treated with 200  $\mu\text{M}$  pirenzepine. WT M3R or M3R<sup>TP/LP</sup> was detected using the anti-HA antibody; the arrow indicates the presumably glycosylated M3R species. The position of the molecular weight standards is indicated to the left. Shown in the bottom panel is a Western blot of the same samples probed for actin as a loading control.

worth mentioning that the pharmacological chaperone effect of pirenzepine was observed only when it was applied above 20  $\mu\text{M}$ . Western blot analysis showed that cells transfected with M3R<sup>TP/LP</sup> did not display a high-molecular mass species (~120 kDa) present in cells expressing WT M3R (Figure 5B). Treatment with antagonists caused the emergence of this ~120 kDa band in M3R<sup>TP/LP</sup>-expressing cells. This band had a fuzzy appearance, which is characteristic of glycosylated proteins. It was shown earlier for other GPCRs that treatment with pharmacological chaperones results in enhanced glycosylation and trafficking of GPCR mutants.<sup>50</sup> Despite the remarkable rescue of M3R<sup>TP/LP</sup> surface expression by atropine, signaling of the mutant remained severely impaired, and it did not respond to CCh (Figure 7) or six other muscarinic agonists (data not shown).

Earlier studies have demonstrated that the abnormally high receptor density in overexpression systems allows M3R to couple to other G proteins, including Gs.<sup>52</sup> To test whether M3R<sup>TP/LP</sup> could activate Gs in transfected CHO-K1 cells, we measured cAMP after cells were treated with atropine to enhance its membrane expression. Forskolin-stimulated cAMP accumulation was similar in cells expressing WT or mutant M3R, regardless of the presence of G $\beta$ 5-RGS7 (Figure 8A). For

WT M3R, CCh-elicited cAMP accumulation had an  $E_{\max}$  that was 85% of the forskolin-stimulated response (Figure 8B). G $\beta$ 5-RGS7 had no effect on  $E_{\max}$  or EC<sub>50</sub>, approximately 10  $\mu\text{M}$ , which were similar to those obtained in the Ca<sup>2+</sup> imaging assay, indicating that the cAMP response was M3R-specific. However, the  $E_{\max}$  for M3R<sup>TP/LP</sup> reached only 10% of that of the WT receptor (Figure 8B). Collectively, our data show that atropine enhances membrane expression of M3R<sup>TP/LP</sup>, and this mutant is capable of binding ligand; however, coupling to both Gq and Gs is nearly abolished.

## DISCUSSION

Understanding how GPCRs interact with accessory proteins is an important area of signal transduction, cell biology, and pharmacology. In this paper, we extend our previous studies investigating the structural basis of the interaction between the G $\beta$ 5-RGS7 complex and M3R. Using a GST pull-down approach, we showed that recombinant fragments of M3R could bind to the G $\beta$ 5-RGS7 complex.<sup>14</sup> Specifically, a central region of the i3 loop spanning amino acids 304–390 bound the recombinant DEP domain of RGS7 with an affinity similar to that of the full-length i3 loop (residues 253–492). Here, we analyzed four i3 loop deletion mutations in the context of the full-length receptor and found that two deletions in the region of residues 304–345 rendered M3R-stimulated Ca<sup>2+</sup> signaling nearly insensitive to G $\beta$ 5-RGS7 regulation (Figure 1). Earlier work showed that the i3 loop of M3R interacts with several proteins, including Gq, G $\beta$  $\gamma$ , calmodulin, and SET, and contains a number of phosphorylation sites.<sup>19,53–56</sup> Our analyses of the region of residues 304–345 did not reveal homology to other proteins or particular structural features, but G $\beta$  $\gamma$  docking and GRK phosphorylation have been mapped to this region.<sup>20</sup> These results suggest that the G $\beta$ 5-RGS7 complex may attenuate M3R-stimulated Ca<sup>2+</sup> signaling by hindering G $\beta$  $\gamma$  docking.

In addition to the i3 loop, our previous studies indicated that the carboxyl terminus of the receptor (M3R CT) is required for interaction with G $\beta$ 5-RGS7. We investigated the importance of two features of M3R CT, the central polybasic stretch, S65-KKKRRK-S70, and helix 8. The polybasic region was implicated in inactive-state preassembly of Gq heterotrimers.<sup>43</sup> Therefore, we hypothesized that G $\beta$ 5-RGS7 could obstruct this mechanism by competing with Gq for this binding site. However, our pull-down data suggest that there may be a complex interaction at this region as Lys-to-Ala substitution weakens DEP but not G $\beta$ 5 interaction (Figure 2). In contrast, we found that amino acid substitutions in helix 8 abolished the interaction with both DEP and G $\beta$ 5 (Figure 2D,E). Helix 8 is a common structural motif present in many GPCRs, which is involved in several processes, including membrane trafficking and G protein recognition and activation.<sup>57–60</sup> Our circular dichroism spectroscopic experiments and molecular dynamics simulations (Figure 3) support our hypothesis that substitution of two helix 8 residues with Pro destabilizes its  $\alpha$ -helical fold. Given that Pro is known to disrupt  $\alpha$ -helices, because of its inability to participate in backbone hydrogen bonding, this result may not be surprising. However, the destabilization of helix 8 with the double Pro substitution became apparent only in a phospholipid environment (Figure 3). The dependence of helix 8 folding on the presence of membrane mimetics was previously observed for peptides from cannabinoid and  $\beta$ 2 adrenergic receptors<sup>61–64</sup> and thus appears to be a common motif among rhodopsin-like GPCRs. Taken together, our

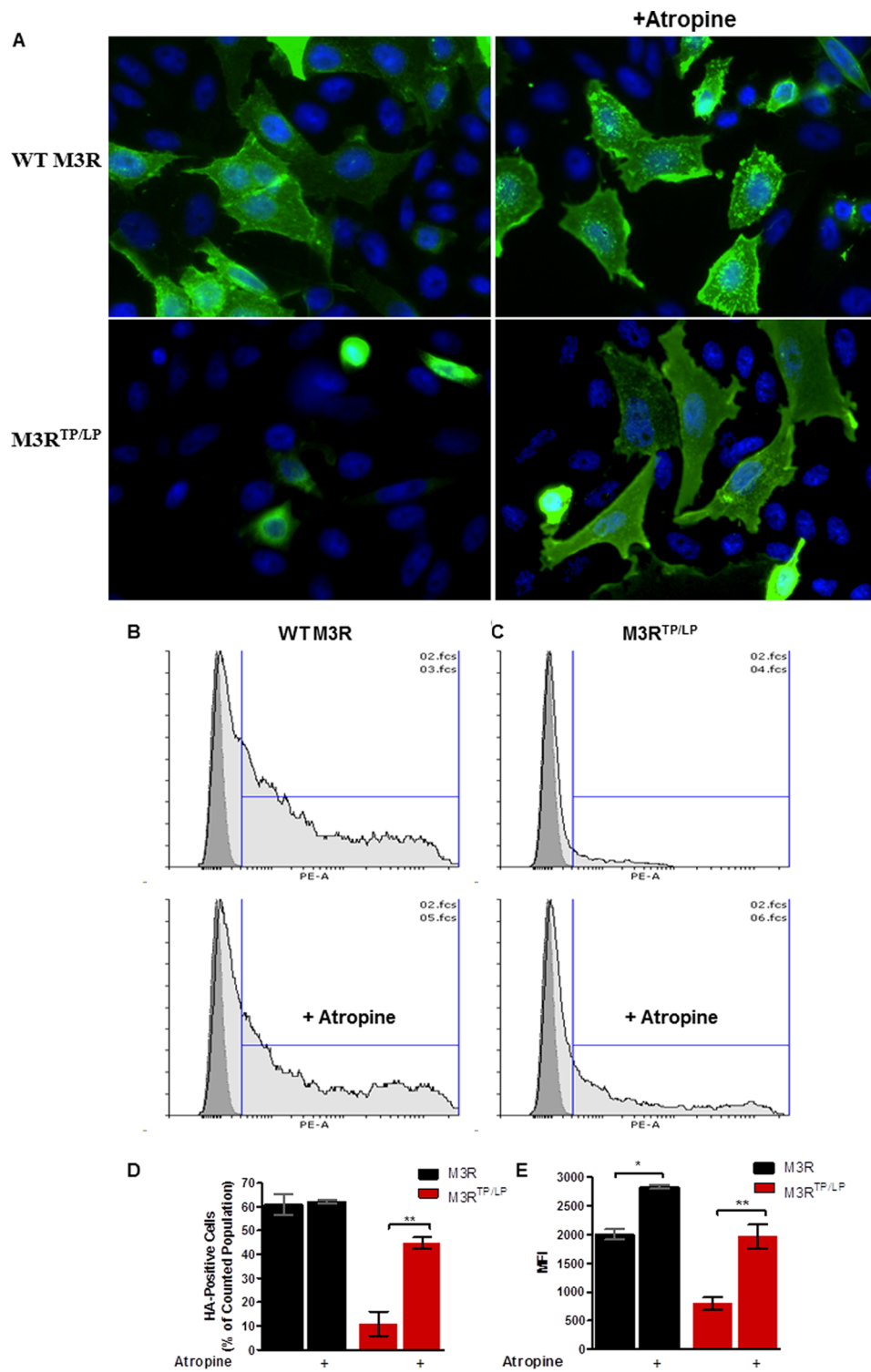


**Figure 6.** Atropine treatment greatly enhances M3R<sup>TP/LP</sup> surface expression. (A) CHO-K1 cells were transfected with M3R or M3R<sup>TP/LP</sup> tagged with the HA epitope at its N-terminus. Forty-eight hours post-transfection, cells were fixed, immunostained under nonpermeabilizing conditions, and analyzed by fluorescence microscopy using a 60× objective lens. Prior to fixation, cells were incubated with 100 nM atropine for 18 h (right panels). Shown are representative images from two independent transfection experiments. (B–D) Cells were detached, labeled with the phycoerythrin-conjugated anti-HA antibody under nonpermeabilizing conditions, and analyzed by flow cytometry as described in Experimental Procedures. Representative histograms for cells transfected with WT M3R (B) or M3R<sup>TP/LP</sup> (C), with or without atropine treatment. The X-axis shows the fluorescence intensity of phycoerythrin and the Y-axis the number of cells. The dark gray peak overlaid on each histogram shows staining of nontransfected CHO-K1 cells used as the negative control. The light gray histogram shows HA-positive transfected cells. Vertical blue lines denote the gate for HA-positive cells. (D) Percent of HA-positive cells in the total counted events. Cells transfected with WT M3R are denoted with black bars and those with the M3R<sup>TP/LP</sup> mutant with red bars [means ± SD ( $n = 2$ )]. (E) Median fluorescence intensity (MFI) of HA-positive cells [means ± SD ( $n = 2$ )].

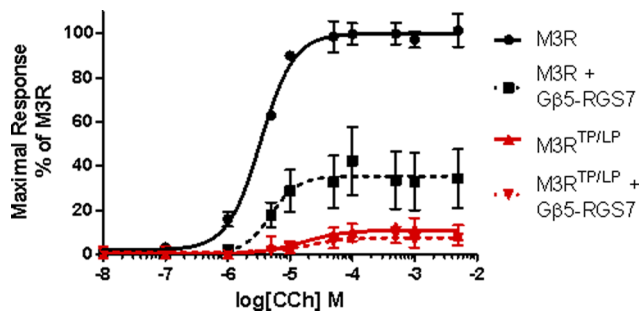


**Figure 7.** Pharmacological chaperoning of M3R<sup>TP/LP</sup> does not restore CCh-stimulated Ca<sup>2+</sup> signaling. Concentration dependency curves of the maximal Ca<sup>2+</sup> release response in atropine-pretreated cells to CCh measured by Fluo-8 fluorescence using FLIPR Tetra in the absence of extracellular Ca<sup>2+</sup>, as described in Experimental Procedures. Cells were transfected with WT M3R (solid black), M3R and Gβ5-RGS7 (dashed black), M3R<sup>TP/LP</sup> (solid red), or M3R<sup>TP/LP</sup> and Gβ5-RGS7 (dashed red). The maximal change in fluorescence intensity of four replicate wells was averaged (means ± SD) and plotted for each concentration of CCh. Curves were fit using the GraphPad Prism 5 sigmoidal dose–response equation with variable slope.

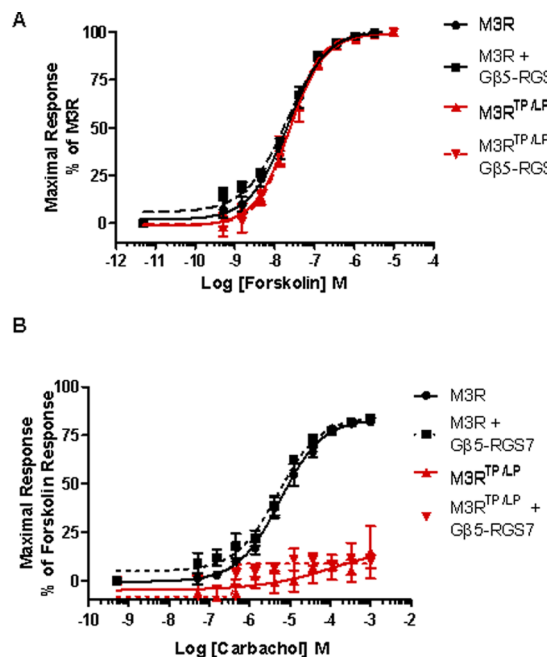


**Figure 8.** Helix 8 mutant of M3R cannot activate Gs. Cells were transfected and treated with atropine as described in the legends of Figures 6 and 7. Forty-eight hours post-transfection, cells were dissociated, seeded, and analyzed for cAMP accumulation using the ULight competitive cAMP immunoassay kit (PerkinElmer) as described in Experimental Procedures. Cells expressing WT M3R (black) or M3R<sup>TP/LP</sup> (red) in the absence (solid) or presence (dashed) of Gβ5-RGS7 were stimulated with increasing concentrations of forskolin (A) or CCh (B). Data are presented as the percent response elicited by 10 μM forskolin-treated cells as 100% control and buffer-treated cells as 0% control according to the formula % response = 100[(negative control) – sample]/[(negative control) – (positive control)]. Each point represents the mean ± SD of four replicate wells, and curves were fit using the sigmoidal nonlinear regression equation with variable slope (GraphPad Prism 5.0).

results indicate that residues 548–567 of the carboxyl terminus of M3R form an α-helix and suggest that its structural integrity is necessary for interaction with Gβ5-RGS7.

In the course of this study, we found that membrane expression of full-length M3R<sup>TP/LP</sup> was severely impaired (Figures 5 and 6). This observation is consistent with previous work on helix 8 mutants of V2R and M1R.<sup>49–51</sup> To improve surface expression, we applied the pharmacological chaperone approach by treating cells with atropine or other antagonists. Despite the dramatic improvement of M3R<sup>TP/LP</sup> membrane expression levels (Figures 5 and 6), its Ca<sup>2+</sup> signaling remained impaired, with the *E*<sub>max</sub> for CCh reaching only 10% of that of WT in the millimolar range of CCh (Figure 7). These functional studies of M3R<sup>TP/LP</sup> did not allow us to probe Gβ5-RGS7 regulation without interfering with G protein coupling. Thus, at the moment, our model in which helix 8 plays a role in sensitizing M3R to Gβ5-RGS7 is based on the GST pull-down studies (Figure 2).

Helix 8 is known to participate in conformational changes that occur upon receptor activation.<sup>29</sup> Recently, we reported that intrinsic properties of muscarinic agonists can determine the sensitivity of M3R to Gβ5-RGS7 regulation.<sup>13</sup> This finding implied that some compounds might stabilize a M3R conformation that is more conducive to Gβ5-RGS7 interaction. Thus, we hypothesized that an agonist other than CCh may overcome the structural instability introduced by the Pro substitutions. However, none of the tested agonists were able to elicit a signal above the CCh response (Figure 7). We also found that the M3R<sup>TP/LP</sup> mutant was incapable of activating another G protein, Gs (Figure 8). These results indicate that the integrity of helix 8 is essential for G protein coupling.

It is worth noting that in the course of our analyses we found that Gβ5-RGS7 does not inhibit the activation of Gs by the overexpressed WT M3R (Figure 8). This overexpression experiment, although superficial, implies that Gβ5-RGS7 selectively inhibits the Gq/PLC pathway. Consistent with our findings, previous biochemical studies revealed that the complex had no effect on AC activity but reduced PLC-β2 activity.<sup>65</sup> Thus, we can speculate that regulation of M3R signaling by Gβ5-RGS7 involves two mechanisms: selective interaction of the complex with M3R and competitive inhibition of PLC-β.

In conclusion, we have demonstrated that the 40 central amino acids in the i3 loop of M3R are necessary for its regulation by the Gβ5-RGS7 complex and found that helix 8 likely plays a role in this interaction. As is the case with other investigated GPCRs, the structural integrity and conformational dynamics of M3R helix 8 are crucial for membrane expression and G protein coupling.

## AUTHOR INFORMATION

### Corresponding Author

\*E-mail: vslepk@med.miami.edu.

### Funding

This work was supported by the National Institutes of Health (Grant GM 060019 to V.Z.S. and Grant GM 083897 to A.F.) and American Heart Association Predoctoral Fellowship 10PRE3600004 to D.K.-S.

### Notes

The authors declare no competing financial interest.

## ACKNOWLEDGMENTS

We thank Qiang Wang and Alexey Pronin for technical advice and helpful suggestions; Deborah Mash, Chun Wu, and Xiaobin Xie for critical assistance with radioligand analysis; and Shaun Brothers and Claes Wahlestedt for providing access to the FLIPR tetra system.

## ABBREVIATIONS

ACh, acetylcholine; CCh, carbachol; CD, circular dichroism; D2R, dopamine D2 receptor; DEP, Disheveled, Egl10, and Pleckstrin homology; DHEX, DEP helical extension; DPC, *n*-dodecylphosphocholine; GAP, GTPase accelerating protein; GGL,  $\gamma$ -like; GPCR, G protein-coupled receptor; GST, glutathione S-transferase; IPTG, isopropyl  $\beta$ -D-1-thiogalactopyranoside; LINCS, linear constraint solver; M2R, muscarinic M2 receptor; M3R, muscarinic M3 receptor; MD, molecular dynamics; Oxo-M, oxotremorine methiodide; PME, particle-mesh Ewald; PBS, phosphate-buffered saline; RGS, regulator of G protein signaling; SD, standard deviation; V2R, vasopressin V2 receptor; WT, wild type; YFP, yellow fluorescent protein.

## REFERENCES

- (1) Rosenbaum, D. M., Rasmussen, S. G., and Kobilka, B. K. (2009) The structure and function of G-protein-coupled receptors. *Nature* 459, 356–363.
- (2) Bockaert, J., Perroy, J., Becamel, C., Marin, P., and Fagni, L. (2010) GPCR interacting proteins (GIPs) in the nervous system: Roles in physiology and pathologies. *Annu. Rev. Pharmacol. Toxicol.* 50, 89–109.
- (3) Willars, G. B. (2006) Mammalian RGS proteins: Multifunctional regulators of cellular signalling. *Semin. Cell Dev. Biol.* 17, 363–376.
- (4) Abramow-Newerly, M., Roy, A. A., Nunn, C., and Chidiac, P. (2006) RGS proteins have a signalling complex: Interactions between RGS proteins and GPCRs, effectors, and auxiliary proteins. *Cell Signalling* 18, 579–591.
- (5) Hollinger, S., and Hepler, J. R. (2002) Cellular regulation of RGS proteins: Modulators and integrators of G protein signaling. *Pharmacol. Rev.* 54, 527–559.
- (6) Witherow, D. S., Wang, Q., Levay, K., Cabrera, J. L., Chen, J., Willars, G. B., and Slepak, V. Z. (2000) Complexes of the G protein subunit  $\beta\gamma$  with the regulators of G protein signaling RGS7 and RGS9. Characterization in native tissues and in transfected cells. *J. Biol. Chem.* 275, 24872–24880.
- (7) Chen, C. K., Eversole-Cire, P., Zhang, H., Mancino, V., Chen, Y. J., He, W., Wensel, T. G., and Simon, M. I. (2003) Instability of GGL domain-containing RGS proteins in mice lacking the G protein  $\beta$ -subunit  $\beta\gamma$ . *Proc. Natl. Acad. Sci. U.S.A.* 100, 6604–6609.
- (8) Jayaraman, M., Zhou, H., Jia, L., Cain, M. D., and Blumer, K. J. (2009) R9AP and R7BP: Traffic cops for the RGS7 family in phototransduction and neuronal GPCR signaling. *Trends Pharmacol. Sci.* 30, 17–24.
- (9) Slepak, V. Z. (2009) Structure, function, and localization of  $\beta\gamma$ -RGS complexes. *Prog. Mol. Biol. Transl. Sci.* 86, 157–203.
- (10) Anderson, G. R., Posokhova, E., and Martemyanov, K. A. (2009) The R7 RGS protein family: Multi-subunit regulators of neuronal G protein signaling. *Cell Biochem. Biophys.* 54, 33–46.
- (11) Celver, J., Sharma, M., and Kovoov, A. (2010) RGS9-2 mediates specific inhibition of agonist-induced internalization of D2-dopamine receptors. *J. Neurochem.* 114, 739–749.
- (12) Orlandi, C., Posokhova, E., Masuho, I., Ray, T. A., Hasan, N., Gregg, R. G., and Martemyanov, K. A. (2012) GPR158/179 regulate G protein signaling by controlling localization and activity of the RGS7 complexes. *J. Cell Biol.* 197, 711–719.
- (13) Karpinsky-Semper, D., Volmar, C. H., Brothers, S. P., and Slepak, V. Z. (2014) Differential Effects of the  $\beta\gamma$ -RGS7 Complex on Muscarinic M3 Receptor-Induced  $\text{Ca}^{2+}$  Influx and Release. *Mol. Pharmacol.* 85, 758–768.
- (14) Sandiford, S. L., Wang, Q., Levay, K., Buchwald, P., and Slepak, V. Z. (2010) Molecular organization of the complex between the muscarinic M3 receptor and the regulator of G protein signaling,  $\beta\gamma$ -RGS7. *Biochemistry* 49, 4998–5006.
- (15) Sandiford, S. L., and Slepak, V. Z. (2009) The  $\beta\gamma$ -RGS7 complex selectively inhibits muscarinic M3 receptor signaling via the interaction between the third intracellular loop of the receptor and the DEP domain of RGS7. *Biochemistry* 48, 2282–2289.
- (16) Narayanan, V., Sandiford, S. L., Wang, Q., Keren-Raifman, T., Levay, K., and Slepak, V. Z. (2007) Intramolecular interaction between the DEP domain of RGS7 and the  $\beta\gamma$  subunit. *Biochemistry* 46, 6859–6870.
- (17) Wess, J. (1996) Molecular biology of muscarinic acetylcholine receptors. *Crit. Rev. Neurobiol.* 10, 69–99.
- (18) Caulfield, M. P. (1993) Muscarinic receptors: Characterization, coupling and function. *Pharmacol. Ther.* 58, 319–379.
- (19) Simon, V., Guidry, J., Gettys, T. W., Tobin, A. B., and Lanier, S. M. (2006) The proto-oncogene SET interacts with muscarinic receptors and attenuates receptor signaling. *J. Biol. Chem.* 281, 40310–40320.
- (20) Wu, G., Bogatkevich, G. S., Mukhin, Y. V., Benovic, J. L., Hildebrandt, J. D., and Lanier, S. M. (2000) Identification of  $\beta\gamma$  binding sites in the third intracellular loop of the M(3)-muscarinic receptor and their role in receptor regulation. *J. Biol. Chem.* 275, 9026–9034.
- (21) Wess, J., Liu, J., Blin, N., Yun, J., Lerche, C., and Kostenis, E. (1997) Structural basis of receptor/G protein coupling selectivity studied with muscarinic receptors as model systems. *Life Sci.* 60, 1007–1014.
- (22) Maggio, R., Barbier, P., Fornai, F., and Corsini, G. U. (1996) Functional role of the third cytoplasmic loop in muscarinic receptor dimerization. *J. Biol. Chem.* 271, 31055–31060.
- (23) Hu, J., Thor, D., Zhou, Y., Liu, T., Wang, Y., McMillin, S. M., Mistry, R., Challiss, R. A., Costanzi, S., and Wess, J. (2012) Structural aspects of M(3) muscarinic acetylcholine receptor dimer formation and activation. *FASEB J.* 26, 604–616.
- (24) Kruse, A. C., Hu, J., Pan, A. C., Arlow, D. H., Rosenbaum, D. M., Rosemond, E., Green, H. F., Liu, T., Chae, P. S., Dror, R. O., Shaw, D. E., Weis, W. I., Wess, J., and Kobilka, B. K. (2012) Structure and dynamics of the M3 muscarinic acetylcholine receptor. *Nature* 482, 552–556.
- (25) Choi, G., Landin, J., and Xie, X. Q. (2002) The cytoplasmic helix of cannabinoid receptor CB2, a conformational study by circular dichroism and  $^1\text{H}$  NMR spectroscopy in aqueous and membrane-like environments. *J. Pept. Res.* 60, 169–177.
- (26) Katragadda, M., Maclejewski, M. W., and Yeagle, P. L. (2004) Structural studies of the putative helix 8 in the human  $\beta 2$  adrenergic receptor: An NMR study. *Biochim. Biophys. Acta* 1663, 74–81.
- (27) Choi, G., Guo, J., and Makriyannis, A. (2005) The conformation of the cytoplasmic helix 8 of the CB1 cannabinoid receptor using NMR and circular dichroism. *Biochim. Biophys. Acta* 1668, 1–9.
- (28) O'Dowd, B. F., Alijaniam, M., Ji, X., Nguyen, T., Eglen, R. M., and George, S. R. (2007) Using ligand-induced conformational change to screen for compounds targeting G-protein-coupled receptors. *J. Biomol. Screening* 12, 175–185.
- (29) Wess, J., Han, S. J., Kim, S. K., Jacobson, K. A., and Li, J. H. (2008) Conformational changes involved in G-protein-coupled-receptor activation. *Trends Pharmacol. Sci.* 29, 616–625.
- (30) Kuwasako, K., Hay, D. L., Nagata, S., Murakami, M., Kitamura, K., and Kato, J. (2013) Functions of third extracellular loop and helix 8 of family B GPCRs complexed with RAMPs and characteristics of their receptor trafficking. *Curr. Protein Pept. Sci.* 14, 416–428.
- (31) Kirchberg, K., Kim, T. Y., Moller, M., Skegrov, D., Raju, G. D., Granzin, J., Buldt, G., Schlesinger, R., and Alexiev, U. (2011) Conformational dynamics of helix 8 in the GPCR rhodopsin controls arrestin activation in the desensitization process. *Proc. Natl. Acad. Sci. U.S.A.* 108, 18690–18695.

- (32) Marti-Renom, M. A., Stuart, A. C., Fiser, A., Sanchez, R., Melo, F., and Sali, A. (2000) Comparative Protein Structure Modeling of Genes and Genomes. *Annu. Rev. Biophys. Biomol. Struct.* 29, 291–325.
- (33) Carson, M. (1991) Ribbons 2.0. *J. Appl. Crystallogr.* 24, 958–961.
- (34) Van Der Spoel, D., Lindahl, E., Hess, B., Groenhof, G., Mark, A. E., and Berendsen, H. J. (2005) GROMACS: Fast, flexible, and free. *J. Comput. Chem.* 26, 1701–1718.
- (35) Lindorff-Larsen, K., Piana, S., Palmo, K., Maragakis, P., Klepeis, J. L., Dror, R. O., and Shaw, D. E. (2010) Improved side-chain torsion potentials for the Amber ff99SB protein force field. *Proteins* 78, 1950–1958.
- (36) Hornak, V., Abel, R., Okur, A., Strockbine, B., Roitberg, A., and Simmerling, C. (2006) Comparison of multiple Amber force fields and development of improved protein backbone parameters. *Proteins* 65, 712–725.
- (37) Toukan, K., and Rahman, A. (1985) Molecular-dynamics study of atomic motions in water. *Phys. Rev. B* 31, 2643–2648.
- (38) Berendsen, H. J. C., Grigera, J. R., and Straatsma, T. P. (1987) The Missing Term in Effective Pair Potentials. *J. Phys. Chem.* 91, 6269–6271.
- (39) Darden, T. A., York, D., and Pedersen, L. (1993) Particle mesh Ewald: An N.log(N) method for Ewald sums in large systems. *J. Chem. Phys.* 98, 10089–10092.
- (40) Hess, B., Bekker, H., Berendsen, H. J. C., and Fraaije, J. G. E. M. (1997) LINCS: A linear constraint solver for molecular simulations. *J. Comput. Chem.* 18, 1463–1472.
- (41) Witherow, D. S., Tovey, S. C., Wang, Q., Willars, G. B., and Slepak, V. Z. (2003) G $\beta$ 5-RGS7 inhibits G $\alpha$ q-mediated signaling via a direct protein-protein interaction. *J. Biol. Chem.* 278, 21307–21313.
- (42) Budd, D. C., Spragg, E. J., Ridd, K., and Tobin, A. B. (2004) Signalling of the M3-muscarinic receptor to the anti-apoptotic pathway. *Biochem. J.* 381, 43–49.
- (43) Qin, K., Dong, C. M., Wu, G. Y., and Lambert, N. A. (2011) Inactive-state preassembly of G(q)-coupled receptors and G(q) heterotrimers. *Nat. Chem. Biol.* 7, 740–747.
- (44) Woody, R. W. (2009) Circular dichroism spectrum of peptides in the poly(Pro)II conformation. *J. Am. Chem. Soc.* 131, 8234–8245.
- (45) Rabanal, F., Ludevid, M. D., Pons, M., and Giralt, E. (1993) CD of proline-rich polypeptides: Application to the study of the repetitive domain of maize glutelin-2. *Biopolymers* 33, 1019–1028.
- (46) Spomer, L., Gertzen, C. G., Schmitz, B., Haussinger, D., Gohlke, H., and Keitel, V. (2014) A membrane-proximal, C-terminal  $\alpha$ -helix is required for plasma membrane localization and function of the G protein-coupled receptor (GPCR) TGR5. *J. Biol. Chem.* 289, 3689–3702.
- (47) Feierler, J., Wirth, M., Welte, B., Schussler, S., Jochum, M., and Faussner, A. (2011) Helix 8 plays a crucial role in bradykinin B(2) receptor trafficking and signaling. *J. Biol. Chem.* 286, 43282–43293.
- (48) Thielen, A., Oueslati, M., Hermosilla, R., Krause, G., Oksche, A., Rosenthal, W., and Schulein, R. (2005) The hydrophobic amino acid residues in the membrane-proximal C tail of the G protein-coupled vasopressin V2 receptor are necessary for transport-competent receptor folding. *FEBS Lett.* 579, 5227–5235.
- (49) Kaye, R. G., Saldanha, J. W., Lu, Z. L., and Hulme, E. C. (2011) Helix 8 of the M1 muscarinic acetylcholine receptor: Scanning mutagenesis delineates a G protein recognition site. *Mol. Pharmacol.* 79, 701–709.
- (50) Morello, J. P., Salahpour, A., Laperriere, A., Bernier, V., Arthus, M. F., Lonergan, M., Petaja-Repo, U., Angers, S., Morin, D., Bichet, D. G., and Bouvier, M. (2000) Pharmacological chaperones rescue cell-surface expression and function of misfolded V2 vasopressin receptor mutants. *J. Clin. Invest.* 105, 887–895.
- (51) Wuller, S., Wiesner, B., Loffler, A., Furkert, J., Krause, G., Hermosilla, R., Schaefer, M., Schulein, R., Rosenthal, W., and Oksche, A. (2004) Pharmacochaperones post-translationally enhance cell surface expression by increasing conformational stability of wild-type and mutant vasopressin V2 receptors. *J. Biol. Chem.* 279, 47254–47263.
- (52) Burford, N. T., Tobin, A. B., and Nahorski, S. R. (1995) Coupling of muscarinic m1, m2 and m3 acetylcholine receptors, expressed in Chinese hamster ovary cells, to pertussis toxin-sensitive/inensitive guanine nucleotide-binding proteins. *Eur. J. Pharmacol.* 289, 343–351.
- (53) Lucas, J. L., Wang, D., and Sadee, W. (2006) Calmodulin binding to peptides derived from the i3 loop of muscarinic receptors. *Pharm. Res.* 23, 647–653.
- (54) Wess, J., Blin, N., Mutschler, E., and Bluml, K. (1995) Muscarinic acetylcholine receptors: Structural basis of ligand binding and G protein coupling. *Life Sci.* 56, 915–922.
- (55) Wu, G., Benovic, J. L., Hildebrandt, J. D., and Lanier, S. M. (1998) Receptor docking sites for G-protein  $\beta\gamma$  subunits. Implications for signal regulation. *J. Biol. Chem.* 273, 7197–7200.
- (56) Simon, V., Oner, S. S., Cohen-Tannoudji, J., Tobin, A. B., and Lanier, S. M. (2012) Influence of the accessory protein SET on M3 muscarinic receptor phosphorylation and G protein coupling. *Mol. Pharmacol.* 82, 17–26.
- (57) Aratake, Y., Okuno, T., Matsunobu, T., Saek, K., Takayanagi, R., Furuya, S., and Yokomizo, T. (2012) Helix 8 of leukotriene B4 receptor 1 inhibits ligand-induced internalization. *FASEB J.* 26, 4068–4078.
- (58) Huynh, J., Thomas, W. G., Aguilar, M. I., and Pattenden, L. K. (2009) Role of helix 8 in G protein-coupled receptors based on structure-function studies on the type 1 angiotensin receptor. *Mol. Cell. Endocrinol.* 302, 118–127.
- (59) Tetsuka, M., Saito, Y., Imai, K., Doi, H., and Maruyama, K. (2004) The basic residues in the membrane-proximal C-terminal tail of the rat melanin-concentrating hormone receptor 1 are required for receptor function. *Endocrinology* 145, 3712–3723.
- (60) Kirchberg, K., Kim, T. Y., Møller, M., Skegro, D., Raju, G. D., Granzin, J., Buldt, G., Schlesinger, R., and Alexiev, U. (2011) Conformational dynamics of helix 8 in the GPCR rhodopsin controls arrestin activation in the desensitization process. *Proc. Natl. Acad. Sci. U.S.A.* 108, 18690–18695.
- (61) Tiburu, E. K., Bowman, A. L., Struppe, J. O., Janero, D. R., Avraham, H. K., and Makriyannis, A. (2009) Solid-state NMR and molecular dynamics characterization of cannabinoid receptor-1 (CB1) helix 7 conformational plasticity in model membranes. *Biochim. Biophys. Acta* 1788, 1159–1167.
- (62) Choi, G., Guo, J., and Makriyannis, A. (2005) The conformation of the cytoplasmic helix 8 of the CB1 cannabinoid receptor using NMR and circular dichroism. *Biochim. Biophys. Acta* 1668, 1–9.
- (63) Katragadda, M., Maciejewski, M. W., and Yeagle, P. L. (2004) Structural studies of the putative helix 8 in the human  $\beta$ (2) adrenergic receptor: An NMR study. *Biochim. Biophys. Acta* 1663, 74–81.
- (64) Choi, G., Landin, J., and Xie, X. Q. (2002) The cytoplasmic helix of cannabinoid receptor CB2, a conformational study by circular dichroism and  $^1$ H NMR spectroscopy in aqueous and membrane-like environments. *J. Pept. Res.* 60, 169–177.
- (65) Posner, B. A., Gilman, A. G., and Harris, B. A. (1999) Regulators of g protein signaling 6 and 7: Purification of complexes with G $\beta$ 5 and assessment of their effects on G protein-mediated signaling pathways. *J. Biol. Chem.* 274, 31087–31093.